In: 2023 AIAA Aviation and Aeronautics Forum and Exposition (AIAA AVIATION Forum)
12-16 June 2023, San Diego, USA
DOI:10.2514/6.2023-3687

# Comprehensive Risk Assessment and Utilization for Contingency Management of Future AAM System

Arinc Tutku Altun*, Yan Xu†, Gokhan Inalhan‡
*Cranfield University, United Kingdom*

Michael W. Hardt§
*Boeing Research and Technology Europe, Spain*

**This paper presents a risk assessment methodology to be used in the future Advanced Air Mobility (AAM) systems especially for supporting the planning phase and onboard contingency management solutions. Two types of dynamic risk maps are introduced as Contingency Risk Map that includes the probability of observing a contingency onboard and Risk Severity Map which covers various sources of data such as population density, a dense air traffic, obstacles, terrain, no-fly zones, and so forth. Contingency Risk Map is to quantify the probability of having a contingency and decide if the quantified probability is above the threshold. If the contingency risk probability is at unacceptable limit, Risk Severity Map assists to select a pre-defined secure emergency landing zone or non-secure emergency landing zone defined onboard. The developed risk assessment structure is tested through two different use cases. First one is about defining locations as vertiport alternatives based on the generated map, in case of a contingency ending up with an AAM vehicle to do emergency landing. Second case considers minimum risk onboard rerouting of an AAM vehicle to a secure/non-secure emergency landing zone under contingency management process. The main objective of this work is to build a system-wide contingency management concept for the AAM system by supporting with UTM services such as risk analysis assistance.**

## I. Introduction

Future Advanced Air Mobility (AAM) is a concept that envisions to transform the current air transportation system into a new transportation system. The new system will provide service to underserved or not-served places such that urban, suburban, and rural areas using high technology vehicles that provide various levels of autonomy. For that purpose, the envisioned AAM system has to satisfy accessibility, flexibility, resiliency, and agility needs of such structure. In order to enable the AAM system's full potential, there are many challenges that have to be considered such as infrastructure, technology, safety, regulations, accessibility, social and environmental impact, and so forth.

Safety is one of the most important challenges to overcome for developing such system. Managing adverse events during operations and providing network-wide safety in case of a contingency/emergency situation are not trivial problems. Therefore, a system-wide contingency management concept has to be developed by assessing network risk levels properly. That concept aims to provide not only network-wide safety but also efficiency by considering contingent vehicle itself and surroundings while dealing with expected or unexpected off-nominal and disruptive events. Figure 1 depicts the system-wide contingency management concept that is considered.

Concept of operations (ConOps) to date for AAM concepts around different parts of the world and from various industry leaders, discuss about contingency and emergency management processes for the envisioned system alongside the operational requirements and concepts, yet contingency management activities are given from vehicle perspective [1–4]. Additionally, autonomous [5] and intelligent [6] contingency management concepts are introduced which emphasizes that aircraft to be aware of both their capabilities and the environment as well as making its own decisions and taking actions. On the other hand, three different autonomy levels for systems are introduced in [4], as automatic, autonomic, and autonomous systems. According to that, contingency management activities are expected to be autonomic systems where predefined solutions are selected autonomously without direct supervision but can be intervened if

*PhD Student, School of Aerospace, Transport and Manufacturing, AIAA Member
†Lecturer in ATM/CNS, School of Aerospace, Transport and Manufacturing, AIAA Member
‡BAE Systems Chair, Professor of Autonomous Systems and Artificial Intelligence, AIAA Associate Member
§Associate Technical Fellow in Airspace Operational Efficiency and Autonomous Operations

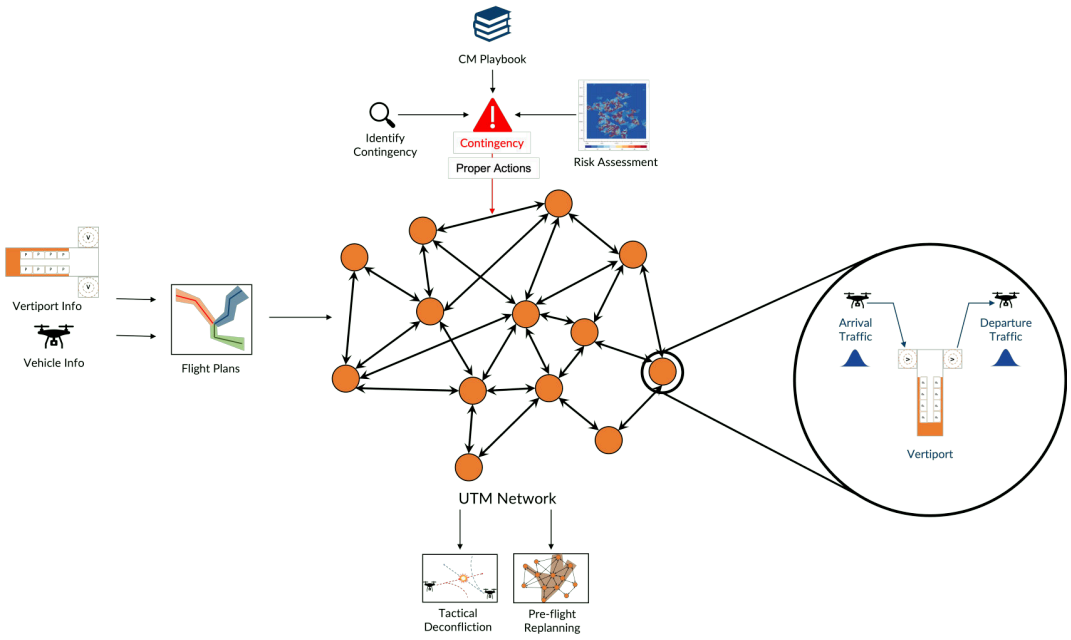


**Fig. 1 Projected contingency management process from the traffic network perspective.**

possible. Moreover, development of a contingency management process onboard for various tactical contingency situations and testing with actual flights, are studied both in the Galician SkyWay project by Boeing Research and Technology Europe [7] and AMU-LED project, by the authors [8]. The considered approaches are mainly from vehicle perspective where it is very useful for resolving contingency cases in a low complexity traffic, yet might not work well in a complex traffic environment which is strongly expected to be the case for AAM system. Therefore, the AAM system requires a system-wide contingency management concept which is defined with base requirements in our previous work [9].

All the Unmanned Aircraft System (UAS) Traffic Management (UTM) services have to cooperate for building the system-wide contingency management concept. This will allow maximizing the traffic's safety as well as providing efficient coordination within the traffic, even in an adverse condition. Risk assessment is one of those crucial UTM services to support contingency management process and create a safer UTM traffic ecosystem by risk-free flight planning, maintaining the flight, and changing trajectories in case of an undesirable situation. Especially, risk maps are very important tools as a decision support system, for selecting safe actions both at strategic and tactical level.

Definition and quantification of the risk metrics to develop a comprehensive risk map is not trivial. There are many research efforts on designing a risk assessment methodology and analysing risk metrics to provide risk analysis assistance to be used for AAM operations. Specific Operational Risk Assessment (SORA) methodology is developed by Joint Authorities for Rulemaking on Unmanned Systems (JARUS) for the evaluation of air and ground risks and determination on the operations to be conducted depending on their risk level [10]. Quantitative approaches are defined by Altiscope to complement and extend the SORA scope and framework and to have a single comprehensive framework [11]. There are also other studies to develop a quantitative background for risk analysis assistance since SORA approach focuses more on the qualitative part in terms of risk categorization. Mathematical basis for risk assessment through a simple probabilistic formalization is introduced and Bayesian network implementation is discussed and compared with SORA in [12] and Bayesian framework is introduced for air risks in [13]. Also, there are risk assessment related studies that are conducted under NASA's System-wide Safety project as in [14–16]. The UTM Risk Assessment Framework (URAF) is designed in [14], by evaluating the risk in real time via Bayesian Belief Networks using vehicle system status, population density, and environmental parameters. Moreover, determination of the non-participant casualty risk level during flights through population density information and onboard sources, is presented in [15] and determination of the obstacle collision risk level by considering off-nominal conditions, is studied in [16]. In [17], probability of fatality is quantified along a flight path by using vehicle specifications, population density, wind, and parameter uncertainties. Static and dynamic ground risk maps are prepared in [18], to be used in offline and online path planning, respectively.

As a continuation of [17, 18], risk map is enhanced by including layers such as population density, height of the ground obstacle, sheltering, and no-fly zone and used for various descent types such that ballistic descent, uncontrolled glide, parachute descent, and fly-away in [19]. Probabilistic risk assessment is studied in [20] by using probabilistic risk exposure map considering risks to people and property on the ground and UAS failure mode analysis. In [21], effects of mid-air collisions and ground risks to human safety are studied by only considering failures at mid-flight phase. In [22], risk cost map is created using probabilistic impact of an accident to pedestrians and ground traffic and is used for flight planning phase. Another study deals with collision risks of flights with people, vehicles, and manned aviation to create risk-free path planning [23]. There is also an onboard flight planning framework that considers optimizing flight time, altitude, and operational risk where operational risk consists of terrain, land usage, obstacles, and airspace restrictions information [24]. The study in [25] focuses on the extension of the third party risks with individual and societal risk indicators in UAS operations. There are other studies that focuses on prediction of risky flight regions due to weather conditions, doing weather hazard risk modeling [26], and predicting the wind behaviour for urban areas [27]. In [28], a risk map is prepared by taking parameters such as casualties, property damage, unmanned aerial vehicle (UAV) survival into account alongside wind and link coverage information and reachability analysis, to be used in parachute landing in case of loss of propulsion. Contingency based risk mapping and relevant uncertainty quantification is studied in [29] for contingency management action selection process for a UAS. Last but not least, in [30, 31], 3-dimensional (3D) risk map is considered based on ground risk aspects such as population, road traffic, ground obstacles, and noise which is used in risk-based 3D path planning. There are many more studies related to UAS ground risk models that are reviewed in [32].

Studies up to date deal with specific aspects of risk map representation mainly considering ground risks through population density and obstacles. Even though the most of the studies show clear representation of the quantification of risk metrics that are considered for a proper risk assessment and minimize the overall risk for operations through flight planning, re-routing; the risk assessment process also has to include a dense UTM traffic which is expected with AAM system and risks associated with off-nominal conditions that can lead to contingency or emergency situations.

In this paper, we are focusing on a risk assessment methodology for UTM through two risk maps which focus on quantification of the contingency risks and risks that can be caused to ground and air. First one is to be used for avoiding contingency possibilities during operations. The probability of any contingency or contingency event combinations occurring is quantified specific to location and timeframe. Second one is for taking proper measures beforehand such as defining safe landing zones or selecting unprepared safe landing locations in case of a contingency situation. Also, that risk map can be used for minimum risk rerouting to the predefined or to be defined safe landing zones. Finally, we aim to validate the concept for vertiport alternatives that is defined under the joint Wisk-Boeing ConOps [4]. Those alternative vertiports are defined for contingency events that may lead an AAM vehicle to do an emergency landing. The given vertiport alternatives consist of diversion vertiports, secure emergency landing zones, and non-secure emergency landing zones where diversion vertiports are vertiports that have capacity for off-nominal landings, secure emergency landing zones are predefined locations that have the proper infrastructure for emergency landings, and non-secure emergency landing zones are risk-free landing areas. The locations of diversion vertiports and secure emergency landing zones must be predefined and non-secure emergency landing zones must be set onboard in case of a contingency, through a proper risk assessment process. On the other hand, rerouting of a flight to those vertiport alternatives must be supported by risk analysis assistance service as well while doing an emergency landing. Our purpose is to support the mentioned contingency management processes in terms of safe landing zone definition/selection and rerouting to that location for emergency landing, via our comprehensive risk assessment methodology.

## II. General Structure

A methodology is developed that deals with generating two separate risk maps to be used both at the pre-operation phase and during the operation. These maps can be named as Contingency Risk Map where the probability of experiencing a contingency situation in each cell of a grid map is given and Risk Severity Map which shows the normalized impact that can be caused by a landing UAS to both ground and air elements. The proposed risk assessment flow is depicted in Figure 2. Once an operation starts, probability of experiencing a contingency is checked with a certain frequency which is quantified via Contingency Risk Map. If the contingency probability exceeds the accepted threshold, then a contingency management action has to be taken which is considered as an emergency landing in this study. Once the operation is updated as contingent, an emergency landing zone has to be selected either as pre-defined diversion vertiport or secure emergency landing zone. Both of these safe landing areas are defined using the Risk Severity Map at pre-flight phase. If these options are not available, a non-secure emergency landing zone has to be picked from the Risk Severity Map which refers to an unprepared safe landing area that is not defined before the operation unlike the other

options. After selecting a safe location to land, the UAS has to be rerouted to that place. For rerouting, Risk Severity Map is used again to minimize the risk that can be caused until completing a safe landing.

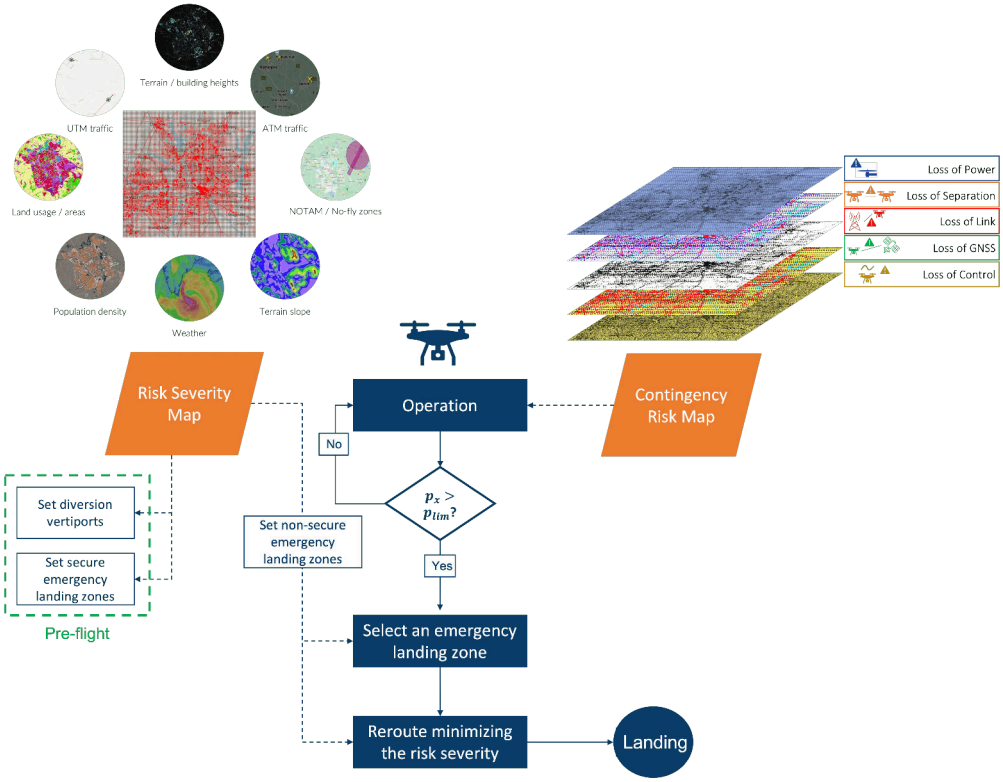


**Fig. 2 General structure of the proposed risk assessment methodology.**

Contingency Risk Map aims to provide information on the type, level, and location of a specific contingency situation that can be expected during operation. That information can be used to minimize the contingency risk for flight planning or change in operation. Additionally, the Contingency Risk Map can also be used as a decision support system for operators or service providers to decide on continuing or terminating the flight depending on the accepted level of contingency risk is exceeded or not. For preparing this map, different contingency sources are modeled such as complete loss or degradation of power, exceeding separation limit with other elements in the network, losing communication link, global positioning system, and control of the UAS.

Risk Severity Map, on the other hand, deals with quantifying the normalized impact that can be made to ground or air elements. It is aimed to be used for defining diversion vertiports and secure emergency landing zones which shall be defined at flight planning or even traffic network planning phase. In case a contingent UAS is not able to use these options due to the location availability or UAS reachability, then a non-secure emergency landing zone option shall be selected via Risk Severity Map. Also, safe rerouting to one of those locations has to be done through the considered map. For generation of the Risk Severity Map, several datasets are considered such that location based population, terrain slope and roughness, infrastructures such as buildings, roads, and airports, current air traffic and expected UAS traffic, and no-fly zones.

Each risk map has a 3D grid map based structure where the cell sizes are customizable depending on the vehicle type. For this study, cell sizes are defined as cubes where the length of each side is 50 m. As given in Figure 3, the area over Dallas/Fort Worth is selected for this research. The area highlighted with blue is focused on for reducing the computational load.

## III. Contingency Risk Map

In this section, various contingency probabilities that are considered for the preparation of the Contingency Risk Map are elaborated. These probabilities refer to the probability of experiencing a specific contingency or a combination

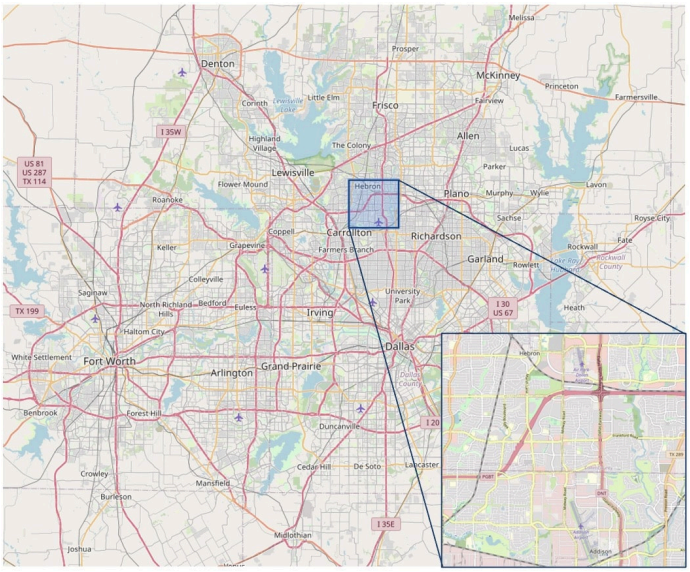


**Fig. 3 Research area of interest, Dallas/Fort Worth.**

of contingencies within a specific cell. Contingency Risk Map is prepared from the specific vehicle's perspective, therefore, it is unique to each operation. The contingencies that are taken into account, are loss of power, loss of separation, loss of link, loss of Global Navigation Satellite System (GNSS), and loss of control.

### A. Loss of Power

Two contributors, propulsion system failure and battery condition, are taken into account as loss of power cases. Propulsion system failures are modeled with a Poisson distribution which allows to quantify the probability of a given number of events occurring within a specific timeframe.

$$P\left(x|\lambda\right) = \frac{1}{x!}\lambda^{x}e^{-\lambda} \tag{1}$$

where $x$ is the number of occurrence of the considered event which is the propulsion system failure and $\lambda$ is the average failure rate of occurrence which is taken as experiencing 1 failure in 2500 flight hours. The obtained probability is dependent to UAS's condition rather than its location. Thus, every cell in the risk map for the considered UAS, is filled with the value obtained from the distribution of the propulsion system failure.

On the other hand, the probabilistic impact of the battery condition is defined with the following probability distribution. Therefore, the probability for losing power is quantified depending on the battery level of the UAS.

$$P(x|b_{critic}) = \begin{cases} e^{-cx/b_{max}}, & \text{if } x \leq b_{critic} \\ 0, & \text{otherwise} \end{cases} \tag{2}$$

where $b_{critic}$ and $b_{max}$ respectively refer to the critical limit and maximum level of the battery in percentage which are 20% and 100%, $x$ is being the current battery level, and $c$ is the scaling coefficient. This distribution is independent from the location of the UAS. Battery condition is the key parameter for quantifying such a probability. Similar with the propulsion system failure, the value observed from the distribution is fed to the every cell in the hypothetical UAS's risk map.

### B. Loss of Separation

Loss of separation can be approached from two perspective as probability of the separation minima violation between ATM traffic and UTM traffic. The focus area includes an active airport, Dallas Addison Airport, that accommodates operations such as charter, corporate, and general aviation flights.

Probability of an AAM vehicle to lose its separation minima with a commercial/general aviation flight or with another AAM vehicle is modeled in a same way as:

$$P(x|d_{conf}, d_{warn}) = \begin{cases} 1, & \text{if } x \leq d_{conf} \\ \left(1 - \dfrac{x - d_{conf}}{d_{warn}}\right)^2, & \text{if } d_{conf} < x \leq d_{warn} \\ 0, & \text{otherwise} \end{cases} \tag{3}$$

where $d_{conf}$ depicts the separation minima and $d_{warn}$ refers to the warning distance. Going from $d_{warn}$ to $d_{conf}$ means increasing the probability of having a loss of separation between other airspace users. In this study, two different distance pairs are used related to ATM and UTM. Yet, conflict and warning distances can be modeled based on the size of the vehicle that is considered for separation. Figure 4a shows a snapshot of the risk map for loss of separation regarding the UTM traffic. The snapshot is taken for the 900 m. altitude which is selected as the operational altitude for the considered UTM traffic. Similarly, Figure 4b depicts the conflict probability with the ATM traffic that lands at the Dallas Addison Airport. Since the aircraft is descending and landing, altitude is selected as 250 m. for the snapshot to clearly capture the distribution and stay within the altitude limit.

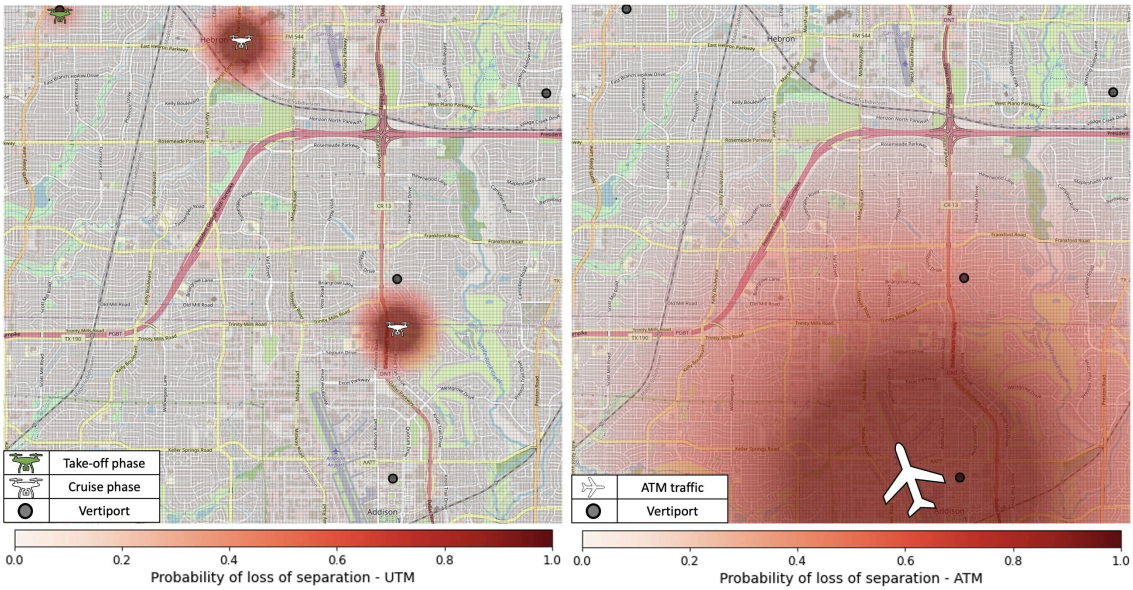


**(a) In a UTM traffic.** **(b) In an ATM traffic.**

**Fig. 4 Snapshot of the map for the probability of having a separation loss.**

### C. Loss of Link

Loss of link case is investigated with three root causes as a failure on the hardware, interruptions on communication, and the link coverage. For modeling the hardware break, Poisson distribution is used similar to the propulsion system failure. The average failure rate of occurrence, $\lambda$, is selected as observing 1 failure for 2000 flight hours. The sampled value is assigned to the every cell of the map generated for the focused UAS. Breakdown of the hardware for providing a link to a UAS may have different impact considering the back-up systems. Thus, the probability of observing loss of link given that there is a hardware failure can be set accordingly.

Communication link interruptions can be caused by different sources such as high winds, thunderstorms/rainstorms, buildings/infrastructures, and cellular traffic. Since there is not any very tall building made out of relatively dense materials over the focus area, the building effect on link interruptions is neglected. Building material and height data is obtained from OpenStreetMap [33]. Similarly, it is assumed that the cellular infrastructure is enough to accommodate high usage rate. Wind effects are studied for quantifying the probability of link interruptions. Wind data is retrieved from National Center for Atmospheric Research, Research Data Archive (NCAR RDA) [34]. Since the resolution of the

wind data is 0.25 degrees and higher data resolution is required, obtained wind data is scaled to the focus area for each altitude level by fitting a Burr distribution to the real wind data and sampling for the focus area.

$$P(x|c,k) = ckx^{c-1}\frac{1}{(1+x^c)^{k+1}} \tag{4}$$

where $c$ and $k$ control the shape and scale of the distribution. Wind data for very low level operations can also be quantified in higher resolution through computational fluid dynamics analysis as in [27]. After obtaining the wind data, the following approach can be followed for quantifying the probability of communication link interruptions.

$$P(x|V_{min},V_{max}) = \begin{cases} 0, & \text{if } x < V_{min} \\ k\dfrac{x-V_{min}}{V_{max}-V_{min}}, & \text{if } V_{min} \le x < V_{max} \\ 1, & \text{otherwise} \end{cases} \tag{5}$$

where $V_{min}$ and $V_{max}$ are the minimum wind speed that creates an interruption and maximum acceptable wind speed, and $k$ is the scaling parameter. A snapshot of the probability of communication interruptions due to wind at 100 m. altitude is given in Figure 5a.

Lastly, for modeling the link coverage, it is assumed that the communication for UASs is provided by using 4G/5G. Thus, a communication coverage model is defined by taking the effective range and performance of the communication towers into account. Communication tower locations are obtained from the OpenStreetMap.

$$P(x|d_{eff},d_{fade},t_p) = \begin{cases} 0, & \text{if } x \le t_p d_{eff} \\ 1-\left(1-\dfrac{x-t_p d_{eff}}{t_p d_{fade}}\right)^2, & \text{if } t_p d_{eff} < x \le t_p d_{fade} \\ 1, & \text{otherwise} \end{cases} \tag{6}$$

where $d_{eff}$ and $d_{fade}$ denote the effective and fading range, $t_p$ represents the performance coefficient of a communication tower. The effective range is picked as 4 km. and the tower performance fades to 7.5 km. In terms of considering the performance of the towers, a performance percentage is introduced that affects the effective and fading ranges. Although, the percentage performance parameter has been set to 100% as a default value, it can be changed for each tower which reduces the tower's effective area. Figure 5b illustrates a snapshot of the probabilities of experiencing loss of link case over each cell due to communication tower coverage limits. A small portion at the south part of the focus area seems to have a possibility for vehicles to experience a loss of link due to coverage.

### D. Loss of GNSS

Loss of GNSS cases are analyzed and modeled from three perspectives. These are GNSS blockage, interference possibility, and GNSS performance depending on the number of satellites that are involved for positioning the UAS.

GNSS blockage may depend on different causes such that cloud formation, building, infrastructures and so forth. The effect of the cloud formation or nominal weather conditions on GNSS performance can be negligible. GNSS blockage due to buildings, on the other hand, can be modeled as follows.

$$\theta_{SAT} = \arcsin\left(\frac{(S_s - S_r)}{\|S_s - S_r\|}\right) \tag{7}$$

where $\theta_{SAT}$ is the elevation angle of the satellite relative to the receiver, $S_s$ and $S_r$ are satellite and receiver position vectors. After obtaining the elevation angle, height of the line of sight can be calculated as below.

$$h_{los} = h_{uas} + dtan(\theta_{SAT}) \tag{8}$$

where $h_{los}$ is the height of the line of sight between the receiver and satellite, $h_{uas}$ is the altitude of the UAS, and $d$ is the horizontal distance between the blockage and the receiver. Therefore, it can be seen that if the signal is blocked or not via the following function.

$$P(x|h_{block}) = \begin{cases} 1, & \text{if } x \le h_{block} \\ 0, & \text{otherwise} \end{cases} \tag{9}$$

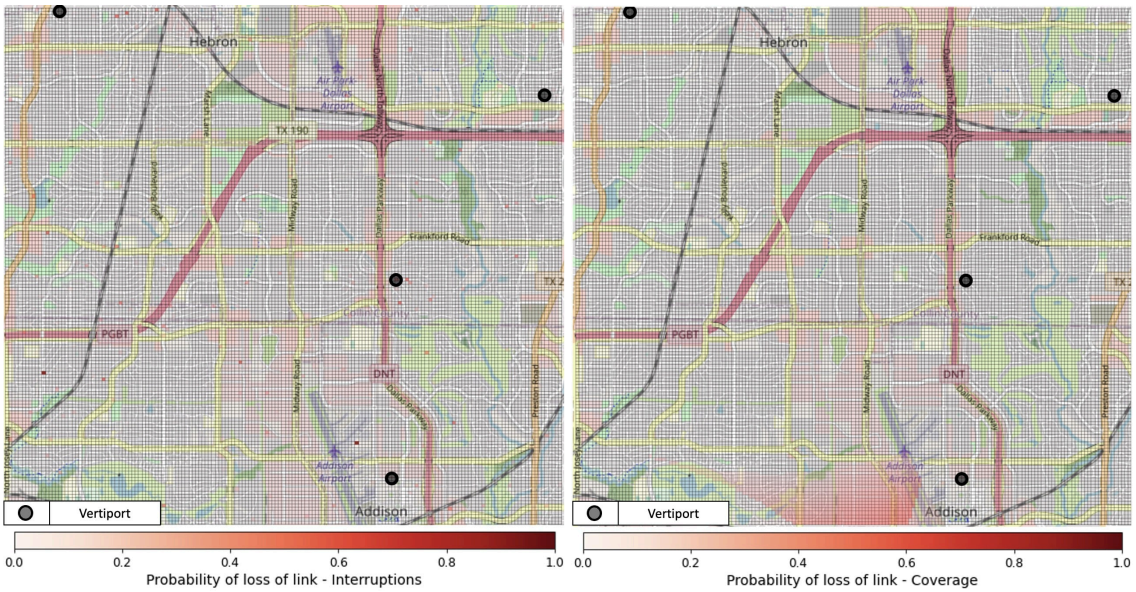


**(a) Link interruptions due to wind.** **(b) Loss of link due to coverage.**

**Fig. 5 Snapshot of the map for the probability of link loss.**

If the height of the blockage, $h_{block}$, is bigger than the height of the line of sight, $x$, that means the signal is blocked. This quantification has to be made for each satellite that can connect with the UAS and average performance has to be defined accordingly. In other words, that probability depends on the location and the elevation angle of each satellite that is connected at that moment. Since the operational altitude is selected as 900 m. for AAM vehicles and there are not very tall buildings in the focus area, GNSS blockage may only be observed at the small portion of the vertical take-off and landing phases. Building height information is extracted from OpenStreetMap by considering building and roof level parameters.

Interference on GNSS can be considered as jamming and spoofing. Signal jamming is overpowering the GPS signal which leads receiver to not operate and signal spoofing misleads GPS receiver to calculate position properly and diverge by giving small disturbances or feeding with fake data. These two activities are considered as a not very frequent event [35], therefore, they are modeled as a Poisson distribution by randomly observing 1 case in 10000 flight hours. This probability is dependent to the location of the jammer or malicious actor, yet, the location of those might not be known properly. Therefore, it is quantified for each cell of the grid map by randomly sampling from the fit distribution.

Lastly, GNSS performance is evaluated with the number of satellites that are connected to the UAS for positioning. The model for the performance of the GNSS based on the number of satellites involved is quantified with a conditional Sigmoid function as below.

$$P(x|n_{min}, n_{suf}) = \begin{cases} 1, & \text{if } x < n_{min} \\ 1 - \dfrac{2}{1 + e^{\frac{n_{suf}-x}{n_{min}}}}, & \text{if } n_{min} \leq x \leq n_{suf} \\ 0, & \text{otherwise} \end{cases} \tag{10}$$

where $n_{min}$ and $n_{suf}$ denote the minimum and sufficient number of satellites required to position the AAM vehicle properly. The minimum number of satellites that are required for roughly positioning the UAS is selected as 4 and the sufficient number of satellites for accurate response is chosen as 8. Figure 6 shows a snapshot from the probability quantification of the number of satellite effects over GNSS performance at the operational altitude. The number of satellites that are connected with the UAS is selected by sampling randomly for each cell.

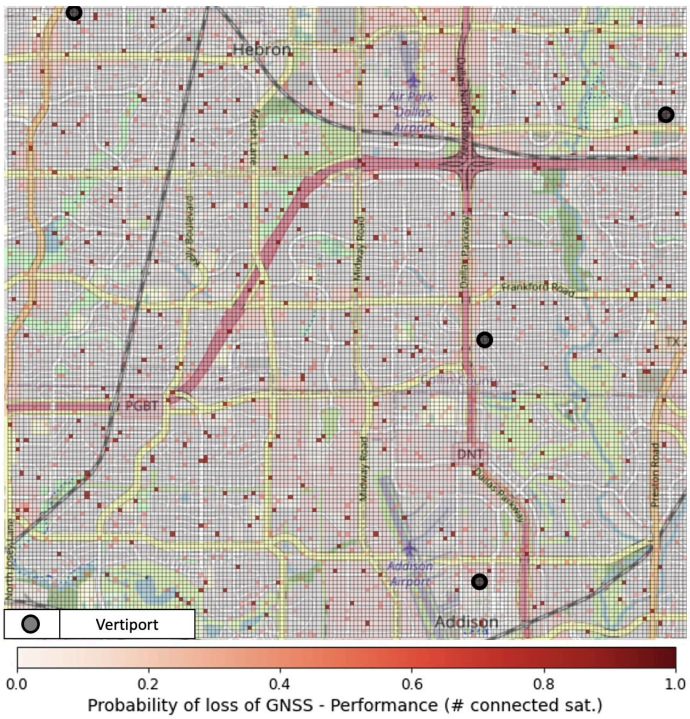


**Fig. 6 Snapshot of the map for the probability of loss of GNSS due to the number of connected satellites.**

### E. Loss of Control

Loss of control case is analyzed considering control system failure and wind effects on a UAS. Control system breakdown is modeled using Poisson distribution same as the other system failures. That type of failure is assumed to be happening once in 3000 flight hours. Similar with the other systems, failure of the control systems depends on the AAM vehicle's condition. Therefore, it is not location dependent and the received output is implemented into the every cell of the vehicle specific contingency risk map.

Also, wind effects are considered for the loss of control cases in an AAM flight. Each vehicle has a certain level of threshold in terms of wind resistance. Once that limit is exceeded, then the probability of observing a control loss may increase depending on the wind severity. Wind data is quantified in a similar way as in the communication link loss case. This situation is modeled as follows.

$$P(x|V_{res}) = \begin{cases} 0, & \text{if } x < V_{res} \\ \dfrac{1}{1 + e^{k\frac{V_{res}-x}{V_{res}}}}, & \text{otherwise} \end{cases} \tag{11}$$

where $V_{res}$ refers to the AAM vehicle's wind resistance and $k$ is the scaling parameter. In this case, wind resistance is taken as 15 m/s for cruise and 8 m/s for vertical take-off and landing phases.

### F. Obtaining the Contingency Risk Map

Contingency Risk Map is generated by combining the probabilistic models for each contingency case. Bayesian network approach which is represented as a directed acyclic graph, is applied for the integration of each condition that leads to a contingency [36, 37]. Nodes of the considered structure represent the individual events and direct edges give the direct causal relationship between nodes. Defining the relationship between variables and their conditional probabilities is one of the most important parts in Bayesian network which can be done considering real data or domain expertise. Figure 7 shows the connection between individual events and their contributors if there is any.

For constructing a joint distribution out of individual and conditional events, the chain rule for the Bayesian networks is used as follows.

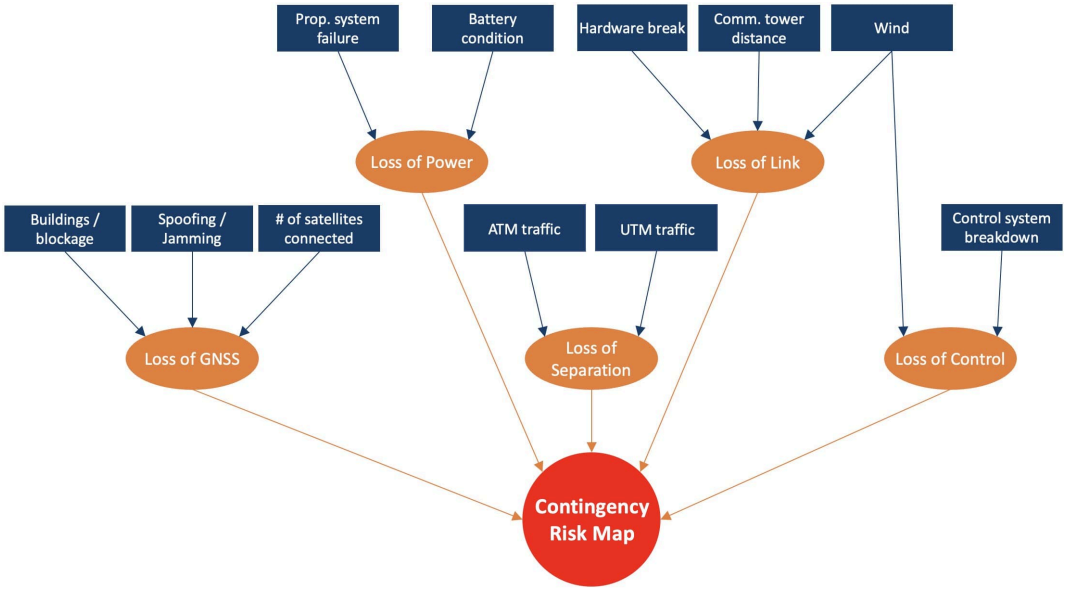


**Fig. 7 Bayesian network for the Contingency Risk Map.**

$$P(x_{1:n}) = \prod_{i=1}^{n} P(x_i | parents(x_i)) \tag{12}$$

where the joint probability $P(x_{i:n})$ is represented by the product of the probabilities of each variable given their parent values and $parents(x_i)$ depicts the particular values of the parent events of $x_i$. Figure 8 shows a snapshot of the obtained Contingency Risk Map which changes over time and has to be updated during operations. The snapshot is taken from the operational altitude.

## IV. Risk Severity Map

This section covers the details of the elements that constitute the Risk Severity Map. The purpose of the Risk Severity Map is to create a baseline for quantifying and normalizing the possible impact of a UAS to the environment in case of a contingency. Generating such a map is beneficial to use for minimizing the expected impact for planning and taking critical actions such as setting diversion vertiports and safe landing zones to be used under an adverse event; selecting an unprepared safe zone due to limited availability at the pre-defined locations; or finding the minimum impact route while taking such actions. Various data sources are considered to obtain the Risk Severity Map. These data sources are population density, ATM and UTM traffic, obstacles, infrastructures, no-fly zones, and terrain.

### A. Population Density

The population density dataset gives information on the people concentration over a specific area which is crucial to locate the crowded locations and avoid them under an emergency condition. Thus, it forms a very important parameter to carefully consider while making decisions using the Risk Severity Map. The population density data used in this work consists of the number of people existing in the 30 m. grid cells. The dataset is retrieved from Facebook Connectivity Lab. [38].

For normalizing the population density data, the following function is used where the maximum number of population can be set by considering the grid sizes of interest, depending on the operator's/UAS's acceptable risk thresholds. Each cell is quantified by this function and the obtained values form the population density map.

$$f_{pd}(x) = \begin{cases} x/N_{max}, & \text{if } x < N_{max} \\ 1, & \text{otherwise} \end{cases} \tag{13}$$

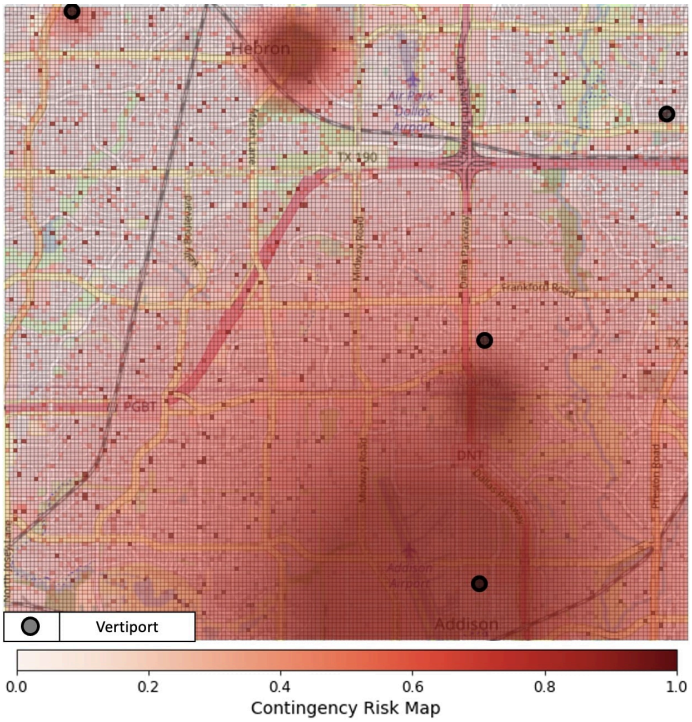


**Fig. 8 Contingency Risk Map.**

where $N_{max}$ denotes the maximum number of people that the considered cell can accommodate. Lowering the $N_{max}$ value means increasing the safety measures over the population. Values are normalized between 0 and 1. Figure 9 shows the population distribution over the focus are in Dallas/Fort Worth.

### B. ATM Traffic

Commercial or general air transportation traffic is a parameter that has to be taken into account while preparing the Risk Severity Map. Since the focus area includes an airport (Dallas Addison Airport) that is still accommodating operations, the current air transportation traffic is included into the map by showing if an aircraft exists in a cell or not.

$$f_{atm}(x) = \begin{cases} 1, & \text{if flight } f \text{ in cell } c \\ 0, & \text{otherwise} \end{cases} \tag{14}$$

ATM traffic data is retrieved from FlightRadar24 [39] where information such as position of the commercial/general aviation flights is used. Figure 10a depicts the traffic that is landing to the Dallas Addison Airport and the instant look of the 250 m. altitude with the occupied cell by the aircraft. Even though the considered airport is not very busy with operations, there are still some elements to care about in terms of risk mapping.

### C. UTM Traffic

UTM traffic is generated by using the vertiport network that is built based on the studies in [40] which analyzes the historical transportation patterns to obtain the possible UTM demand trend for Dallas/Fort Worth area. The network covers information such as vertiport locations and capacities. As a vehicle model, a lift and cruise type (Wisk Cora) vehicle is used for the whole traffic which has around 177 km/h cruise speed, 20 km/h vertical speed, 100 km range, and 19 minutes maximum flight time [41]. The range and endurance limits of the chosen vehicle are considered for obtaining the feasible origin-destination (O/D) pairs. After these parameters are obtained, the UTM traffic network is built by using the current ATM traffic network as a basis to create a logical demand pattern between vertiports by capturing the behaviour between high-demand airports. The built UTM traffic is included into the Risk Severity Map in a similar way as for the ATM traffic.

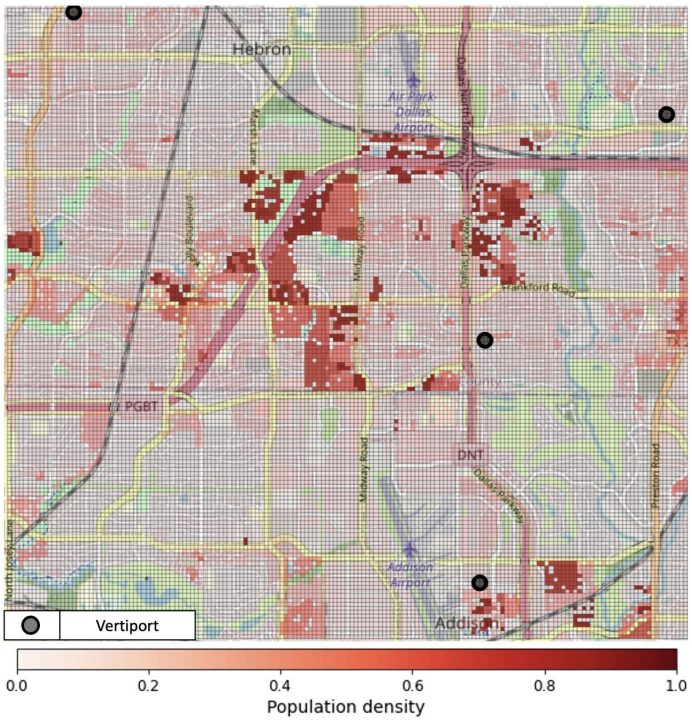


**Fig. 9 Population density map.**

$$f_{utm}(x) = \begin{cases} 1, & \text{if flight } f \text{ in cell } c \\ 0, & \text{otherwise} \end{cases} \tag{15}$$

The generated UTM traffic for a day and a snapshot for 900 m. altitude over the focus area to see the instant occupied cells for the risk map, are represented in Figure 10b. The traffic network consists of 75 vertiports as nodes and 18349 direct routing flights as edges.

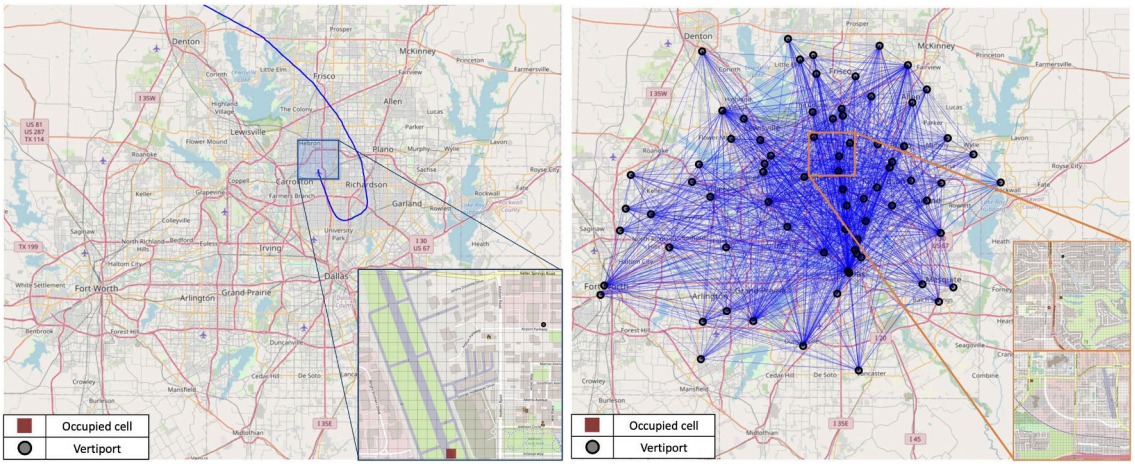


**(a) ATM traffic and its full trajectory.** **(b) Generated UTM traffic and its full trajectories.**

**Fig. 10 Snapshot of the air traffic network.**

### D. Area Usage

Land usage is an important source which assists for analyzing the possible damage on infrastructures and landing UASs. Residential areas, buildings, roads, railways, airports, and areas covered by water are the datasets that are considered for building the area usage map. Those datasets are retrieved from OpenStreetMap. Figure 11a shows the land usage over the focus area. Buildings including heights for 3D mapping, roads, and railways are given in red, airports are given in yellow, and water areas are given in blue. Buildings, roads, railways, airports, infrastructures are both damageable and can cause damage to UAS. Watery areas, on the other hand, are considered as not suitable for landing since the UAS can be lost or broken due to such a landing.

### E. No-fly Zones

No-fly zones are modeled as cylinders where a UAS cannot go through. No-fly zone function is modeled where the area and the affected altitude levels can be customized.

$$f_{nofly}(x) = \begin{cases} 1, & \text{if cell } c \text{ within no-fly zone } A_{nofly} \\ 0, & \text{otherwise} \end{cases} \tag{16}$$

where $A_{nofly}$ represents the volume that is picked as a no-fly zone and $c$ depicts the individual cell in the 3D grid map. Figure 11b shows an example of a no-fly zone.

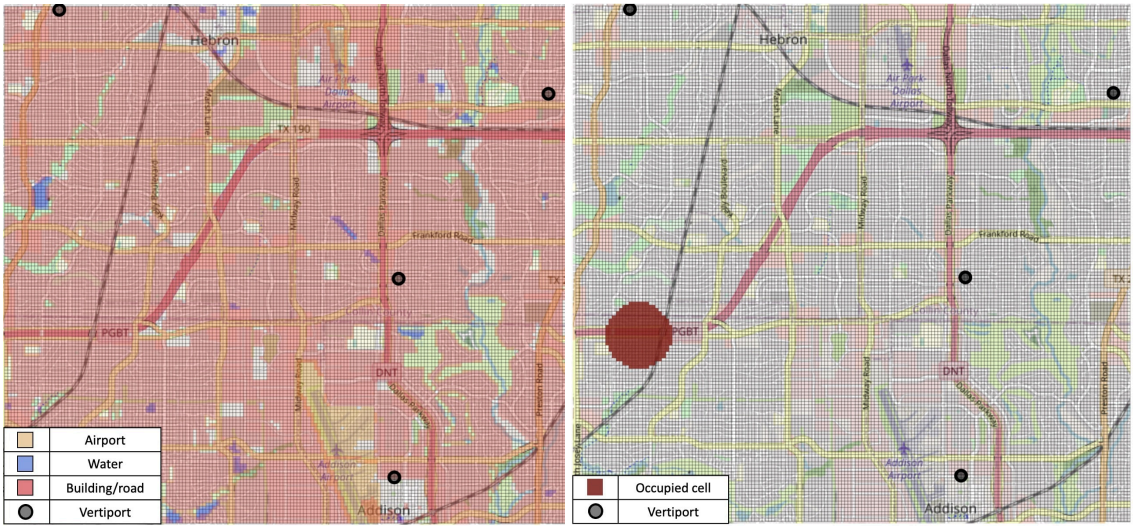


**(a) Area usage.** **(b) No-fly zone.**

**Fig. 11 Snapshot of the area usage and no-fly zone.**

### F. Terrain

Terrain slope and roughness are considered for selecting a proper, smoother safe places to land for a UAS. Digital elevation data is retrieved from United States Geological Survey (USGS) [42]. The approach in [28] is followed for modeling these two parameters. For terrain slope, singular value decomposition is used to fit a plane to the real data and obtain the slope angle of the terrain plane. After that, the obtained slope angles are normalized and filtered based on the UAS's acceptable slope limit which is denoted as $\theta_{max}$. Figure 12a shows the terrain slope map of the focus area.

$$f_{slope}(x) = \begin{cases} x/\theta_{max}, & \text{if } x < \theta_{max} \\ 1, & \text{otherwise} \end{cases} \tag{17}$$

Similar to the terrain slope, roughness of the surface for each cell is calculated by taking the standard deviation of the elevation data. An acceptable limit of roughness is considered that is given as $\sigma_{max}$. Figure 12b depicts the roughness map of the focus area.

$$f_{rough}(x) = \begin{cases} x/\sigma_{max}, & \text{if } x < \sigma_{max} \\ 1, & \text{otherwise} \end{cases} \tag{18}$$

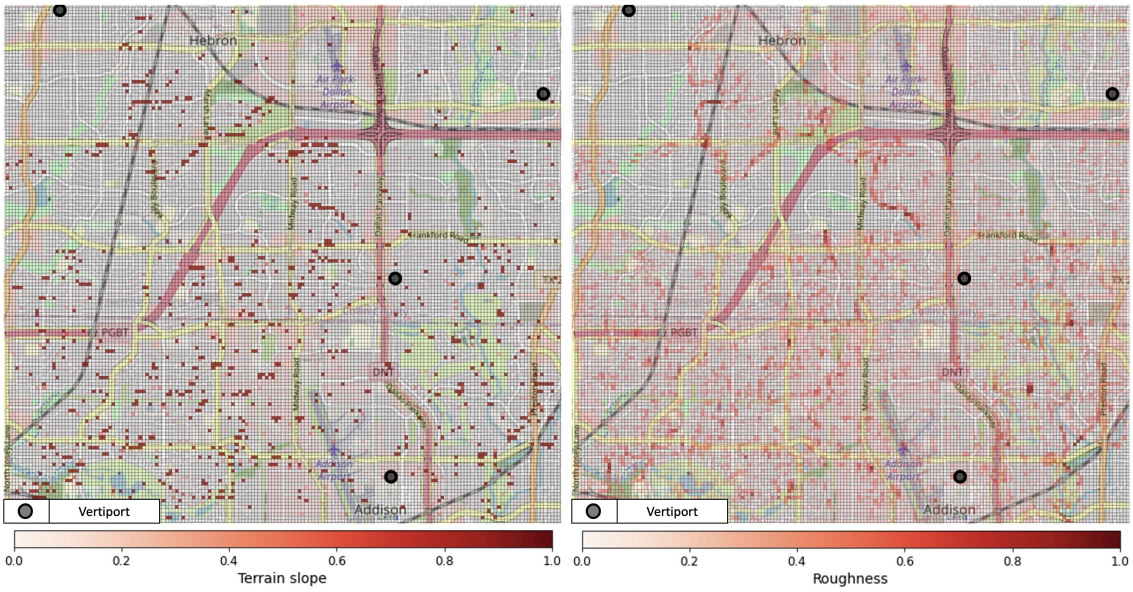


**(a) Terrain slope.** **(b) Surface roughness.**

**Fig. 12 Risk map based on terrain related parameters.**

Finally, the terrain risk severity map is obtained by summing up the terrain slope and roughness parameters. The parameters are weighted equally.

$$f_{terrain}(x) = 0.5 f_{slope}(x) + 0.5 f_{rough}(x) \tag{19}$$

### G. Obtaining the Risk Severity Map

Risk Severity Map is achieved by integrating the data sources that are explained. For the integration, cumulative value of each data is considered along with the weights assigned. Table 1 shows the data structures and weights assigned to each map obtained through the aforementioned datasets. Represented weights can be updated depending on the operation type, operational area, and purpose of the operator/service provider. Weights can also be selected based on time since the considered Risk Severity Map has a dynamic nature.

**Table 1 Risk Severity Map structure**

| Data | Structure | Importance % |
|---|---|---|
| Population density | Static | 35 |
| ATM traffic | Dynamic | 20 |
| UTM traffic | Dynamic | 20 |
| Area usage | Static | 10 |
| No-fly zones | Dynamic | 10 |
| Terrain (for landing surface) | Static | 5 |

Let $R^t$ be the grid map at time $t$ for one of the datasets where each cell is filled with $f(x_{i,j})$.

$$R^t = \begin{bmatrix} f(x_{1,1}) & \dots & f(x_{1,m}) \\ \vdots & \ddots & \vdots \\ f(x_{n,1}) & \dots & f(x_{n,m}) \end{bmatrix} \tag{20}$$

After obtaining the each grid map from the data sources $R = \{R_{pd}, R_{atm}, R_{utm}, R_{area}, R_{nofly}, R_{terrain}\}$ and using the weights defined $w = \{w_{pd}, w_{atm}, w_{utm}, w_{area}, w_{nofly}, w_{terrain}\}$, Risk Severity Map can be created via a weighted sum of the each risk contributor as follows.

$$RSM = \sum_{i=1}^{6} w_i R_i \tag{21}$$

Figure 13 depicts a snapshot of the Risk Severity Map built at ground level. Risk Severity Map is a 3D map where various data sources such as population, ATM/UTM data, no-fly zones, land usage considering heights of the infrastructures, and terrain related parameters.

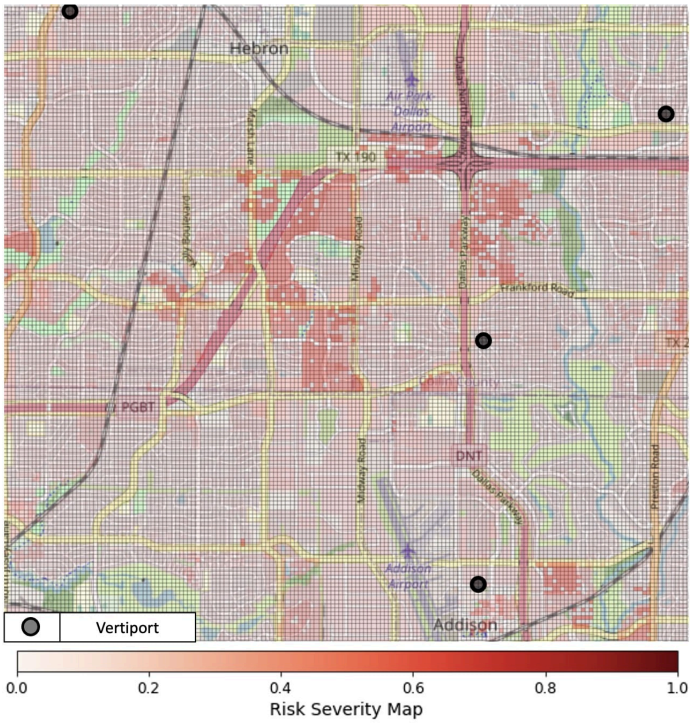


**Fig. 13 Risk severity map.**

## V. Case Studies

There are two case studies that are considered for utilizing the introduced risk assessment process. The main focus of the case studies is the concept defined under the joint Wisk-Boeing ConOps [4] which deals with setting secure emergency landing zones at pre-flight phase and deciding on non-secure emergency landing zones onboard if necessary. After observing possible safe locations, risk minimizing rerouting after a contingency situation case is elaborated.

### A. Defining Secure/Non-secure Emergency Landing Zones

For setting the diversion vertiports and defining the secure/non-secure emergency landing zones, Risk Severity Map can be used. First, an acceptable level of risk shall be defined either by the operator or service provider. Diversion vertiports are existing vertiports that can reduce the risk level of a contingency situation by having a capacity to allow a

contingent vehicle to do emergency landing. Secure emergency landing zones are defined as safe landing spots that are set and designed with an infrastructure that can accommodate emergency landings and non-secure emergency landing zones are landing places that have an acceptable level of risk. Non-secure emergency landing zones can be used in case the other options are not available or suitable. Figure 14a and 14b show the safe areas for different risk thresholds. The green areas can be used to define secure emergency landing zones at the infrastructure planning phase. Once they are set, the rest of the places can be used as non-secure emergency landing zones during operations.

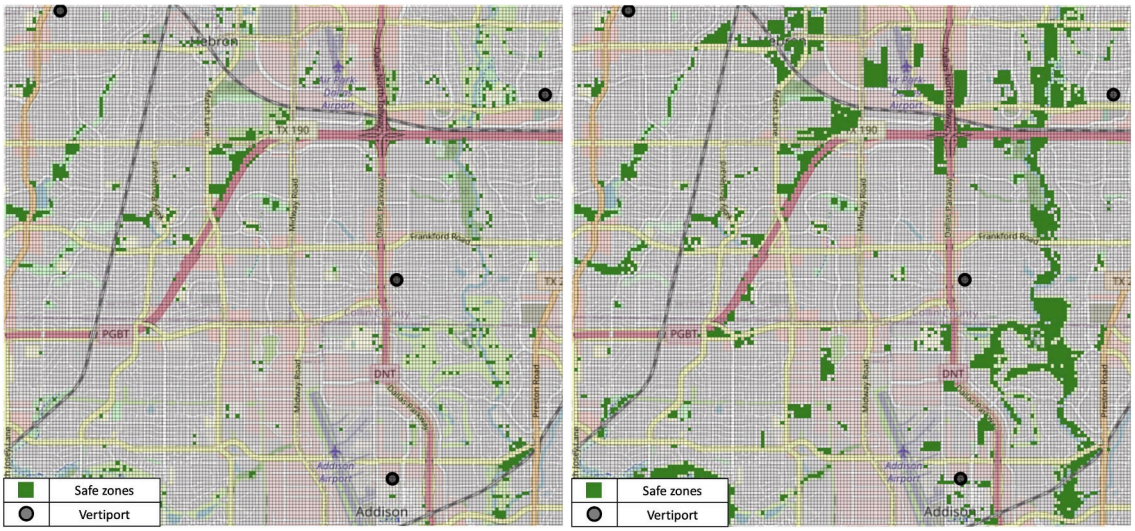


**(a) Threshold: no risk.** **(b) Threshold: 2% risk.**

**Fig. 14 Snapshot of the Risk Severity Map with different limits of the accepted risk.**

For our case studies, the weight of the terrain parameter is relatively small. Therefore, the reason for the increase in the number of green cells in 2% risk threshold compared to the no risk threshold is the terrain related parameters such as roughness and terrain slope. These parameters refer to the smoothness of the landing zone. As it can be seen in Figure 14, some parts of the parks/green areas are enabled for defining safe landing zones.

### B. Risk Minimum Emergency Routing

After defining the secure emergency landing zones, we focused on minimum risk rerouting problem in case of an emergency landing. If the contingency probability of the cell that contains our operation is above the UAS's contingency probability limit, then the UAS takes an emergency landing action to one of the secure (pre-defined) or non-secure (defined onboard) emergency landing zones. Contingency probability limit of an operation refers to a safety buffer for taking proper measures before a contingency occurs. This buffer can be defined either by the operator or service provider.

In Figure 15, the considered UAS checks the flight's contingency probability through the Contingency Risk Map and receives a probability that is above the operation's safety threshold. Therefore, the UAS takes an emergency landing action towards the closest (based on the Euclidean distance) and available secure emergency landing zone that is defined prior to operation. The action includes a risk minimum rerouting to the selected spot. For that purpose, A* algorithm is used for finding the safest and shortest path [43]. Rerouting is done by considering the Risk Severity Map, where all the altitude layers are combined. The purpose of that is to avoid risks at the current altitude level of the contingent UAS, as well as preventing the UAS from passing over populated areas and critical infrastructures while executing an emergency landing.

## VI. Conclusion

In this paper, we presented a comprehensive risk assessment methodology by considering contingency possibilities that can be faced during flights and risk severity to surroundings after a contingency breaks out. Contingency Risk Map and Risk Severity Map are introduced as parts of this methodology. These dynamic maps are obtained by

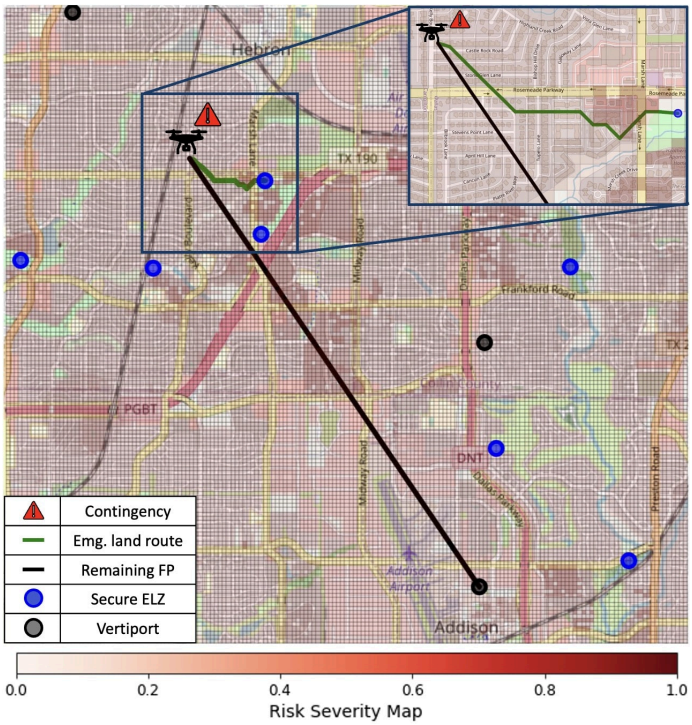


**Fig. 15 Risk minimum emergency landing flight path.**

analyzing probabilistic models for contingency occurrences and using relevant datasets for the surroundings to consider, respectively. Methodology checks the probability of experiencing a contingency onboard through the Contingency Risk Map, depending on the UAS's location and situation. If the contingency probability is above the threshold defined for the specific flight, then the flight falls into the contingent situation and takes an emergency landing action to a safe zone. That safe zone is set either as the closest diversion vertiport or secure emergency landing zone which are defined at pre-tactical phase through the Risk Severity Map. If none of these options are available, UAS takes an action towards a non-secure emergency landing zone which is defined onboard. Additionally, rerouting of the flight to the selected landing spot is also made via the Risk Severity Map.

As a future work, we plan to refine the probabilistic models that we introduced with more realistic data and transform some of the static datasets into dynamic such as population density by considering it through daily (work/school hours), weekly (weekdays/weekends), monthly (summer/winter) basis, and special events. Also, new methods for representing the Contingency Risk Map and Risk Severity Map will be explored. Lastly, the usage area of the introduced risk methodology will be extended for the actions that are taken through relevant UTM services such as tactical and pre-tactical conflict resolution.

## Acknowledgments

Arinc Tutku Altun is funded by Boeing Research and Technology Europe under the Engineering and Physical Sciences Research Council (EPSRC) Doctoral Training Programme (DTP) for the research project entitled Contingency Management of the Advanced Air Mobility System of Systems: UAS/UAM, Integrated ATM/UTM and Infrastructures.

## References

[1] Federal Aviation Administration NextGen, "Urban air mobility (UAM) concept of operations v1.0," Tech. rep., 2020.

[2] CORUS, "U-space concept of operations ed 03.00.02," Tech. rep., SESAR JU, 2019.

[3] Airservices Australia and Embraer Business Innovation Center, "Urban air traffic management concept of operations v1.0," Tech. rep., 2020.

[4] Wisk and Boeing, "Concept of operations for uncrewed urban air mobility," Tech. rep., 2022.

[5] Price, G., Dougles, H., Jenkins, K., Kvicala, M., Parker, S., and Wolfe, R., "Urban air mobility operational concept (OpsCon) passenger-carrying operations," Tech. rep., NASA, 2019.

[6] Gregory, I. M., Campbell, N. H., Neogi, N. A., Holbrook, J. B., Grauer, J. A., Bacon, B. J., Murphy, P. C., Moerder, D. D., Simmons, B. M., Acheson, M. J., et al., "Intelligent contingency management for urban air mobility," *International Conference on Dynamic Data Driven Application Systems*, Springer, 2020, pp. 22–26.

[7] Vidal-Franco, I., Hardt, M., Ruiz, M., Romay, E., Costa, J., Alfonsin, M., Ballesteros, I., Romero, A., Navarro, E., and Larrosa, A., "Robust UAS communications and loss of link operational impact," *2021 IEEE/AIAA 40th Digital Avionics Systems Conference (DASC)*, IEEE, 2021, pp. 1–10.

[8] AMU-LED, "Disruption management framework for non-nominal operations affecting the operator D3.4," Tech. rep., SESAR JU, 2022.

[9] Altun, A. T., Xu, Y., Inalhan, G., Vidal-Franco, I., and Hardt, M., "Contingency management concept generation for U-space system," *2022 Integrated Communication, Navigation and Surveillance Conference (ICNS)*, IEEE, 2022, pp. 1–12.

[10] Joint Authorities for Rulemaking on Unmanned Systems, "JARUS guidelines on specific operations risk assessment (SORA) v2.0," Tech. rep., 2019.

[11] Sachs, P., "A quantitative framework for UAV risk assessment v1.0," Tech. rep., Altiscope ($A^3$ by Airbus), 2018.

[12] Denney, E., Pai, G., and Johnson, M., "Towards a rigorous basis for specific operations risk assessment of UAS," *2018 IEEE/AIAA 37th Digital Avionics Systems Conference (DASC)*, IEEE, 2018, pp. 1–10.

[13] Martin, T., Huang, Z. F., and McFadyen, A., "Airspace risk management for UAVs a framework for optimising detector performance standards and airspace traffic using JARUS SORA," *2018 IEEE/AIAA 37th Digital Avionics Systems Conference (DASC)*, IEEE, 2018, pp. 1516–1525.

[14] Ancel, E., Capristan, F. M., Foster, J. V., and Condotta, R. C., "Real-time risk assessment framework for unmanned aircraft system (UAS) traffic management (UTM)," *17th AIAA Aviation Technology, Integration, and Operations Conference*, 2017, p. 3273.

[15] Ancel, E., Capristan, F. M., Foster, J. V., and Condotta, R. C., "In-time non-participant casualty risk assessment to support onboard decision making for autonomous unmanned aircraft," *AIAA Aviation 2019 Forum*, 2019, p. 3053.

[16] Banerjee, P., Gorospe, G., and Ancel, E., "3D representation of UAV-obstacle collision risk under off-nominal conditions," *2021 IEEE Aerospace Conference (50100)*, IEEE, 2021, pp. 1–7.

[17] la Cour-Harbo, A., "Quantifying risk of ground impact fatalities for small unmanned aircraft," *Journal of Intelligent & Robotic Systems*, Vol. 93, No. 1, 2019, pp. 367–384.

[18] Primatesta, S., Guglieri, G., and Rizzo, A., "A risk-aware path planning Strategy for UAVs in urban environments," *Journal of Intelligent & Robotic Systems*, Vol. 95, No. 2, 2019, pp. 629–643.

[19] Primatesta, S., Rizzo, A., and la Cour-Harbo, A., "Ground risk map for unmanned aircraft in urban environments," *Journal of Intelligent & Robotic Systems*, Vol. 97, No. 3, 2020, pp. 489–509.

[20] Kaya, U. C., Dogan, A., and Huber, M., "A probabilistic risk assessment framework for the path planning of safe task-aware UAS operations," *AIAA Scitech 2019 Forum*, 2019, p. 2079.

[21] Lum, C., and Waggoner, B., "A risk based paradigm and model for unmanned aerial systems in the national airspace," *Infotech@ Aerospace 2011*, 2011, p. 1424.

[22] Su, Y., and Xu, Y., "Risk-based flight planning and management for urban air mobility," *AIAA Aviation 2022 Forum*, 2022, p. 3619.

[23] Hu, X., Pang, B., Dai, F., and Low, K. H., "Risk assessment model for UAV cost-effective path planning in urban environments," *IEEE Access*, Vol. 8, 2020, pp. 150162–150173.

[24] Schopferer, S., and Benders, S., "Minimum-risk path planning for long-range and low-altitude flights of autonomous unmanned aircraft," *AIAA Scitech 2020 Forum*, 2020, p. 0137.

[25] Blom, H. A., Jiang, C., Grimme, W. B., Mitici, M., and Cheung, Y. S., "Third party risk modelling of Unmanned Aircraft System operations, with application to parcel delivery service," *Reliability Engineering & System Safety*, Vol. 214, 2021, p. 107788.

[26] Roseman, C. A., and Argrow, B. M., "Weather hazard risk quantification for sUAS safety risk management," *Journal of Atmospheric and Oceanic Technology*, Vol. 37, No. 7, 2020, pp. 1251–1268.

[27] Jeong, S., You, K., and Seok, D., "Hazardous flight region prediction for a small UAV operated in an urban area using a deep neural network," *Aerospace Science and Technology*, Vol. 118, 2021, p. 107060.

[28] Bleier, M., Settele, F., Krauss, M., Knoll, A., and Schilling, K., "Risk assessment of flight paths for automatic emergency parachute deployment in UAVs," *IFAC-PapersOnLine*, Vol. 48, No. 9, 2015, pp. 180–185.

[29] Escudero, N., "Contingency manager agent for safe UAV autonomous operations," , 2020. AA228-Decision Making under Uncertainty course project.

[30] Pang, B., Hu, X., Dai, W., and Low, K. H., "UAV path optimization with an integrated cost assessment model considering third-party risks in metropolitan environments," *Reliability Engineering & System Safety*, Vol. 222, 2022, p. 108399.

[31] Pang, B., Hu, X., Dai, W., and Low, K. H., "Third party risk modelling and assessment for safe UAV path planning in metropolitan environments," *arXiv preprint arXiv:2107.01834*, 2021.

[32] Washington, A., Clothier, R. A., and Silva, J., "A review of unmanned aircraft system ground risk models," *Progress in Aerospace Sciences*, Vol. 95, 2017, pp. 24–44.

[33] Open Street Map contributors, "Land usage data," , 2017. Data retrieved from, `https://export.hotosm.org/en/v3/exports/new/select/treetag`.

[34] National Centers for Environmental Prediction, National Weather Service, NOAA, U.S. Department of Commerce, "NCEP GFS 0.25 Degree Global Forecast Grids Historical Archive," , 2015. Research Data Archive at the National Center for Atmospheric Research, Computational and Information Systems Laboratory, `https://doi.org/10.5065/D65D8PWK` Accessed 7 April 2023.

[35] GPSJam, "Daily Maps for GPS Interference," , 2006. `https://gpsjam.org/?lat=32.88703&lon=-96.98688&z=9.3&date=2023-02-16` Accessed 20 April 2023.

[36] Neapolitan, R. E., *Probabilistic reasoning in expert systems: theory and algorithms*, John Wiley & Sons, Inc., 1990.

[37] Stephenson, T. A., "An introduction to Bayesian network theory and usage," Tech. rep., Idiap, 2000.

[38] Facebook Connectivity Lab and Center for International Earth Science Information Network - CIESIN - Columbia University, "High Resolution Settlement Layer (HRSL)," , 2016. Source imagery for HRSL © 2016 DigitalGlobe. Accessed 12 February 2023.

[39] FlightRadar24, "Live Flight Tracker," , 2006. `https://www.flightradar24.com/32.96,-96.83/13` Accessed 25 March 2023.

[40] Rimjha, M., Li, M., Hinze, N., Tarafdar, S., Hotle, S., Swingle, H., Trani, A., and Smith, J. C., "Demand forecast model development and scenarios generation for urban air mobility concepts," 2020.

[41] Howard, R. J., Wright, E., Mudumba, S. V., Gunady, N. I., Sells, B. E., and Maheshwari, A., "Assessing the suitability of urban air mobility vehicles for a specific aerodrome network," *AIAA Aviation 2021 Forum*, 2021, p. 3208.

[42] United States Geological Survey (USGS), "Shuttle Radar Topography Mission (SRTM) 1 Arc-Second Global," , 2000. `https://doi.org/10.5066/F7PR7TFT` Accessed 22 April 2023.

[43] Hart, P. E., Nilsson, N. J., and Raphael, B., "A formal basis for the heuristic determination of minimum cost paths," *IEEE transactions on Systems Science and Cybernetics*, Vol. 4, No. 2, 1968, pp. 100–107.

2023-06-08

# Comprehensive risk assessment and utilization for contingency management of future AAM system

Altun, Arinc Tutku

AIAA

Altun AT, Xu Y, Inalhan G, Hardt MW. (2023) Comprehensive risk assessment and utilization for contingency management of future AAM system. In: 2023 AIAA Aviation and Aeronautics Forum and Exposition (AIAA AVIATION Forum), 12-16 June 2023, San Diego, USA. Paper number AIAA 2023-3687

https://doi.org/10.2514/6.2023-3687